Biogeosciences, 11, 4753–4770, 2014
www.biogeosciences.net/11/4753/2014/
doi:10.5194/bg-11-4753-2014
© Author(s) 2014. CC Attribution 3.0 License.

Biogeosciences Open Access

Assessing effects of permafrost thaw on C fluxes based on multiyear modeling across a permafrost thaw gradient at Stordalen, Sweden

J. Deng[1], C. Li[1], S. Frolking[1], Y. Zhang[2], K. Bäckstrand[3], and P. Crill[3]

[1]Earth Systems Research Center, Institute for the Study of Earth, Oceans and Space, University of New Hampshire, 39 College Road, Durham NH 03824, USA
[2]Canada Centre for Mapping and Earth Observation, Natural Resources Canada, 588 Booth Street, Ottawa ON K1A 0Y7, Canada
[3]Department of Geological Sciences, Stockholm University, 106 91 Stockholm, Sweden

Correspondence to: C. Li (cs_li_98@yahoo.com)

Received: 3 February 2014 – Published in Biogeosciences Discuss.: 11 March 2014
Revised: 27 July 2014 – Accepted: 1 August 2014 – Published: 9 September 2014

Abstract. Northern peatlands in permafrost regions contain a large amount of organic carbon (C) in the soil. Climate warming and associated permafrost degradation are expected to have significant impacts on the C balance of these ecosystems, but the magnitude is uncertain. We incorporated a permafrost model, Northern Ecosystem Soil Temperature (NEST), into a biogeochemical model, DeNitrification-DeComposition (DNDC), to model C dynamics in high-latitude peatland ecosystems. The enhanced model was applied to assess effects of permafrost thaw on C fluxes of a subarctic peatland at Stordalen, Sweden. DNDC simulated soil freeze–thaw dynamics, net ecosystem exchange of CO_2 (NEE), and CH_4 fluxes across three typical land cover types, which represent a gradient in the process of ongoing permafrost thaw at Stordalen. Model results were compared with multiyear field measurements, and the validation indicates that DNDC was able to simulate observed differences in seasonal soil thaw, NEE, and CH_4 fluxes across the three land cover types. Consistent with the results from field studies, the modeled C fluxes across the permafrost thaw gradient demonstrate that permafrost thaw and the associated changes in soil hydrology and vegetation not only increase net uptake of C from the atmosphere but also increase the annual to decadal radiative forcing impacts on climate due to increased CH_4 emissions. This study indicates the potential of utilizing biogeochemical models, such as DNDC, to predict the soil thermal regime in permafrost areas and to investigate impacts of permafrost thaw on ecosystem C fluxes after incorporating a permafrost component into the model framework.

1 Introduction

Northern peatlands are characterized by cold and wet conditions that promote the accumulation of soil organic carbon (SOC) (e.g., T. Johansson et al., 2006; Schuur et al., 2008). These ecosystems have accumulated 473–621 Pg (10^{15} g) carbon (C) since the Last Glacial Maximum (Yu et al., 2010), with more than 277 Pg C stored in permafrost areas (Schuur et al., 2008; Tarnocai et al., 2009). Although northern peatlands have generally acted as sinks of carbon dioxide (CO_2) in the past and in the current climate (e.g., Lund et al., 2010; McGuire et al., 2009), peat C stocks may be released into the atmosphere with climate warming, due to mobilization of previously frozen C in permafrost soils and accelerated decomposition of SOC (e.g., Frolking et al., 2011; McGuire et al., 2009; Schuur et al., 2009, 2011). In addition, because of prevailing anaerobic soil conditions, northern peatlands are an important source of atmospheric methane (CH_4), releasing 31–65 Tg CH_4 yr^{-1} (McGuire et al., 2009) and methane emissions can change with permafrost thaw (Christensen et al., 2004).

Pronounced warming has been observed in northern high latitudes, with surface air temperature increased by approximately 0.09 °C $decade^{-1}$ during the 20th century (ACIA, 2005). More pronounced warming has been projected in this region for the 21st century (IPCC, 2007). Many recent studies have argued that the rate or extent of permafrost degradation is increasing with climate warming in northern peatlands (e.g., James et al., 2013; Payette et al., 2004; Quinton et al.,

2011; Åkermanand Johansson, 2008). Permafrost thaw can result in increases in active layer thickness (ALT; the thickness of surface soil layer that freezes and thaws seasonally above a year-round frozen layer) and cause land surface subsidence, which in turn may cause changes in topography, soil hydrology, and vegetation (e.g., Avis et al., 2011; M. Johansson et al., 2006; Schuur et al., 2008). These changes associated with permafrost degradation can significantly affect the C cycle in northern ecosystems (e.g., Dorrepaal et al., 2009; T. Johansson et al., 2006; McGuire et al., 2009; Schneider von Diemling et al., 2012).

Although much concern has been placed on the C balance in permafrost ecosystems, large uncertainty still exists (e.g., Koven et al., 2011; McGuire et al., 2009; Schuur et al., 2011). Northern peatlands are highly heterogeneous, usually with varying characteristics of permafrost, topography, hydrology, soil, and vegetation within close proximity (Nungesser, 2003), which results in considerable variations of C fluxes at local and landscape scales (e.g., Bäckstrand et al., 2010; Lund et al., 2010; Sachs et al., 2010). Responses of the C balance to permafrost degradation have been shown to vary across different peatlands as well (Bäckstrand et al., 2010). Therefore, it is an ongoing challenge to extrapolate site-specific measurements to large regions.

Process-based models are effective tools to assess the impacts of climate change on boreal ecosystems. Several large-scale models have been enhanced by incorporating thermal, hydrologic, vegetation, and biogeochemical processes in relation to permafrost conditions and these models have been applied to quantify the impacts of climate change on C fluxes at regional and global scales (e.g., Schneider von Diemling et al., 2012; Wania et al., 2009a, b; Zhuang et al., 2001, 2004, 2006). Predictions by large-scale models are generally done at coarse spatial resolutions, and therefore they may be deficient in considering the effects of local spatial heterogeneity. By improperly considering fine-scale spatial heterogeneity in vegetation and environmental conditions, systematic biases may occur in simulations of permafrost degradation and C fluxes (Bohn and Lettenmaier, 2010; Zhang et al., 2013). In addition, the results based on coarse-scale modeling are difficult to validate by comparing with field observations and uncertainty may arise in regional and global simulations due to limited validation (Kirschke et al., 2013).

A process-based biogeochemical model, DeNitrification-DeComposition (DNDC), was recently enhanced by incorporating a permafrost model, Northern Ecosystem Soil Temperature (NEST), for predicting biogeochemistry in high latitudes from plant communities to ecosystem scale. The model was initially tested against one growing season of CH_4 flux data measured at a permafrost site in the Lena River delta, Russia (Zhang et al., 2012). In this study, we applied the enhanced model to assess effects of permafrost thaw on C fluxes of a well-studied subarctic peatland at Stordalen, Sweden. The study peatland is located in a discontinuous permafrost zone and consists of palsas – small, relatively dry plateaus elevated 1 to a few meters due to subsurface ice lenses (Williams and Smith, 1989) – and intervening low, wetter areas. These palsas can expand and shrink in extent with relatively small variations in environmental conditions such as temperatures or winter snow packs (Payette et al., 2004), and represent one class of permafrost (Davis, 2001). Stordalen's palsas are extremely vulnerable to changing climate and widespread degradation of permafrost is expected to occur (Åkerman and Johansson, 2008). DNDC simulated multiyear soil freeze–thaw dynamics, net ecosystem exchange (NEE) of CO_2, and CH_4 fluxes across three typical land cover types, which represent a gradient of permafrost degradation in the study region. During simulations, different soil hydrologic conditions and vegetation characteristics of these land cover types were used as model inputs; therefore we focused on predicting the changes in soil thermal dynamics and C cycling along with thawing. The model was tested against long-term field measurements to verify its applicability for simulating the differences in the soil thermal regime and C fluxes across a gradient of permafrost thaw. Then we assessed the possible impacts of permafrost thaw on C fluxes for the Stordalen peatland based on the multiyear simulations. A validated simulation model provides a mechanism for not only interpreting observations but also predicting the impacts of future climate change on greenhouse gas emissions.

2 Methods and data

2.1 The study area and field observations

The study area is the Stordalen mire (68° 20′ N, 19°03′ E; 351 m a.s.l.) located 10 km southeast of Abisko Scientific Research Station (ANS) in northern Sweden. It is a subarctic peatland with discontinuous permafrost. Peat formation at the mire occurred at about 5000 cal BP (Rosswall et al., 1975; Kokfelt et al., 2010). This area has a continental climate, with an annual mean air temperature of 0.07 °C and an average annual precipitation of 308 mm from 1986 to 2006 according to the observations at ANS (Callaghan et al., 2010). Long-term climate records at ANS indicate that the annual mean air temperature in this region has increased by 2.5 °C from 1913 to 2006, significantly exceeding the 0 °C threshold for the first time during the last few decades (Bäckstrand et al., 2008; Callaghan et al., 2010). This warming has led to a thicker active layer and permafrost disappearance in this area (Åkerman and Johansson, 2008). The degradation of permafrost has significantly affected surface topography, hydrology, and vegetation and thereby exerted a strong influence on the fluxes of CO_2 and CH_4 (Christensen et al., 2004; T. Johansson et al., 2006; Malmer et al., 2005; Åkerman and Johansson, 2008).

As in most peatlands in permafrost regions, Stordalen mire has high spatial heterogeneity in topography (1–2 m relative

differences in elevation). The topographic variability creates small-scale (meters) environments with different soil moisture and nutrient conditions that support different plant communities (Rosswall et al., 1975; Bäckstrand et al., 2008). The area can be broadly classified into three typical land cover types (i.e., dry palsa, semiwet sphagnum, and wet eriophorum; note that in this study the terms sphagnum and eriophorum indicate land cover types instead of vegetation species). The palsa sites of Stordalen are dry features underlain by permafrost, with an ALT usually < 0.7 m in late summer; the sphagnum sites are also underlain by permafrost, representing intermediate thaw features, with an ALT generally thicker than 1.0 m in late summer, and are wetter than the palsa with water table levels fluctuating close to the ground surface; the eriophorum sites have no permafrost and are generally wetter than sphagnum, with water table levels constantly near or above the ground surface (Bäckstrand et al., 2008, 2010; Olefeldt and Roulet, 2012). They are also differentiated by elevation, with palsa being highest, sphagnum intermediate, and eriophorum lowest. Therefore these three land cover types have different permafrost regimes and soil water conditions, which support different vegetation compositions (Bäckstrand et al., 2008, 2010). During the last three decades, there have been pronounced shifts in the extent of these three land cover types, with palsa being converted into *Sphagnum*- or *Eriophorum*-dominated land cover in the northern part of the Stordalen mire and both palsa and sphagnum being converted into *Eriophorum*-dominated land cover in the southern part of the mire (Christensen et al., 2004; Malmer et al., 2005). These three land cover types can be regarded as representing a gradient of permafrost degradation (e.g., Malmer et al., 2005; T. Johansson et al., 2006; Bäckstrand et al., 2010).

CO_2 and CH_4 fluxes were measured using automated chambers at Stordalen from 2003 to 2009. NEE was measured at three sites (i.e., the palsa, sphagnum, and eriophorum sites) to represent three typical land cover types, and CH_4 emissions were consistently observed at the sphagnum and eriophorum sites, where water table levels were above or near the peat surface (Bäckstrand et al., 2008, 2010). The palsa site is relatively dry and its CH_4 flux is near zero (Bäckstrand et al., 2008). For each plot, an autochamber system measured CO_2 and total hydrocarbon (THC) fluxes every 3 h, and there were eight measurements per day. CH_4 fluxes were manually observed approximately three times per week by taking samples from every chamber and these measurements were used to quantify the proportion of CH_4 in the measured THC (Bäckstrand et al., 2008, 2010). Daily NEE and CH_4 fluxes were calculated as average values of eight measurements. From 2003 to 2009, valid rates of daily NEE were calculated for 85–213 days in a year based on the field measurements. Daily CH_4 fluxes were available for 79–116 days in a year, with an exception in 2006 when the instrument was down (Bäckstrand et al., 2008, 2010). In addition, soil thaw depth (measured to 90 cm) and water table depth (WTD) were measured 3–5 times per week from early May to mid-October each year (Bäckstrand et al., 2008). Daily meteorological data, including air temperature, precipitation, solar radiation, wind speed, as well as relative humidity, were recorded at the ANS (Fig. 1). The technical details regarding the measurements of NEE and CH_4 fluxes, and the relevant auxiliary variables were described by Bäckstrand et al. (2008, 2010).

2.2 Modification of DNDC

2.2.1 Overview of the DNDC model

DNDC is a process-based model developed for quantifying C sequestration as well as the emissions of carbon and nitrogen (N) gases from terrestrial ecosystems (Li et al., 1992a, b, 2000; Stange et al., 2000; Zhang et al., 2002). The model has incorporated a relatively complete suite of biophysical and biogeochemical processes, which enables it to compute the complex transport and transformations of C and N in terrestrial ecosystems under both aerobic and anaerobic conditions.

DNDC is comprised of six interacting submodels: soil climate, plant growth, decomposition, nitrification, denitrification, and fermentation. The soil climate, plant growth, and decomposition submodels convert the primary drivers, such as climate, soil properties, vegetation, and anthropogenic activity, into soil environmental factors, such as soil temperature and moisture, pH, redox potential (Eh), and substrate concentrations. The nitrification, denitrification, and fermentation submodels simulate C and N transformations that are mediated by soil microbes and controlled by soil environmental factors (Li, 2000; Li et al., 2012). In DNDC, NEE is calculated as the difference between net primary production (NPP) and soil microbial heterotrophic respiration (HR). NPP is simulated at a daily time step by considering the effects of several environmental factors on plant growth, including radiation, air temperature, soil moisture, and N availability. The model simulates the production of plant litter and incorporates the plant litter into pools of soil organic matter (SOM). HR is calculated by simulating decomposition of SOM. SOM is divided into four pools in DNDC, namely litter, microbes, humads, and passive humus. Each pool is further divided into two or three subpools with specific C to N (C / N) ratios and decomposition rates. As a microbially mediated process, decomposition of each SOM fraction depends on its specific decomposition rate as well as soil thermal and moisture conditions (Li et al., 2012). Methane flux is predicted by modeling CH_4 production, oxidation, and transport processes. CH_4 production is simulated by calculating substrate concentrations (i.e., electron donors and acceptors) resulting from decomposition of SOC as well as plant root activities including exudation and respiration, and then by tracking a series of reductive reactions between electron donors (i.e., H_2 and dissolved organic carbon) and acceptors

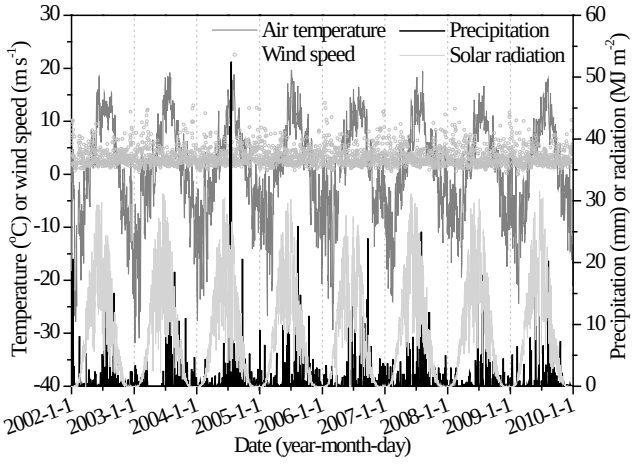

Figure 1. Daily average air temperature, wind speed, precipitation, and solar radiation from 2002 to 2009. Data were recorded at Abisko Scientific Research Station (ANS).

(i.e., NO_3^-, Mn^{4+}, Fe^{3+}, SO_4^{2-}, and CO_2). In DNDC, CH_4 production and oxidation can occur simultaneously within a soil layer but within relatively aerobic and anaerobic microsites, whose volumetric fractions are defined by an Eh calculator, a so-called "anaerobic balloon", embedded in the model framework (Li, 2007). Redox potential, temperature, and pH, along with the concentrations of electron donors and acceptors, are the major factors controlling the rates of CH_4 production and oxidation. CH_4 is transported from soil into atmosphere via plant-mediated transport, ebullition, and diffusion (Fumoto et al., 2008; Zhang et al., 2002).

2.2.2 Soil freeze–thaw and permafrost dynamics

Traditionally, DNDC simulated the soil thermal dynamics by means of a relatively simple module without detailed processes describing the soil thermal regime in the presence of permafrost. It did not explicitly simulate energy exchange within soil–vegetation–atmosphere system, snowpack thermal dynamics, the presence of permafrost, or active layer dynamics (Zhang et al., 2002). However, these processes or environmental factors are important for characterizing the permafrost regime, soil thermal dynamics, soil hydrology, or C and N cycles in high latitudes (e.g., Riseborough et al., 2008; Waelbroeck, 1993). In order to make DNDC more suitable for northern ecosystems, especially frozen soil conditions, we incorporated a permafrost model, NEST, into the model framework (Zhang et al., 2012). NEST is a process-based model which simulates ground thermal dynamics, soil freeze–thaw dynamics, and permafrost conditions (Zhang et al., 2003). In NEST, soil temperature and the permafrost thermal regime are calculated by solving the heat conduction equation, with the upper boundary condition determined by surface energy balance and the lower boundary condition being defined as the geothermal heat flux. The effects of climate, vegetation, snow pack, ground features, and hydrological conditions on the soil thermal regime are incorporated into the model on the basis of energy and water exchanges within soil–vegetation–atmosphere system (Zhang et al., 2003, 2005). To ensure that DNDC simulates permafrost environmental factors and biogeochemistry in synchrony, NEST's functions, which describe soil thermal and hydrologic regimes, were embedded into the framework of DNDC at the model code level. After coupling to NEST, DNDC was able to simulate both the seasonal dynamics of active layer and the long-term variations of permafrost as well as their impacts on biogeochemical processes (Zhang et al., 2012). Therefore, the model should better serve investigations of impacts of climate change on C fluxes in high-latitude ecosystems.

2.3 Model application

We performed DNDC simulations for the three typical Stordalen land cover types (palsa, sphagnum, and eriophorum) from 2002 to 2009. Daily meteorological data (i.e., maximum, mean, and minimum air temperature, precipitation, solar radiation, wind speed, and humidity) from 2002 to 2009 recorded at the ANS were collected to support the simulations. All sites had a surface soil layer of peat (0.5 m) overlying a silt soil layer (Rosswallet al., 1975; Rydeńet al., 1980; Olefeldtet al., 2012). The peat had a bulk density of $0.15\,g\,cm^{-3}$, SOC content of $0.5\,kg\,C\,kg^{-1}$ SDW (soil dry weight), total porosity of 0.9, field capacity of 0.4 (water-filled pore space), wilting point of 0.15 (water-filled pore space), and pH (H_2O) of 5.0, according to observations from Malmer and Walleń (1996), Rydeń et al. (1980), and Öquist and Svensson (2002). The local bedrock is granite (Rosswallet al., 1975) and a thermal conductivity of $2.9\,W\,m^{-1}\,°C^{-1}$ was used (Clauser and Huenges, 1995). The geothermal heat flux in the study region was estimated to be $0.06\,W\,m^{-2}$ (Majorowicz and Wybraniec, 2011).

While the three land cover types share common conditions regarding weather, geology, and soil during the simulations, they differ in soil hydrologic conditions and vegetation characteristics. In order to predict the dynamics of water table at the sphagnum and eriophorum sites, DNDC used several parameters to estimate lateral flows, including surface inflow rate, maximum water table depths for surface and ground outflows, and surface and ground outflow rates (Zhang et al., 2002). We estimated these parameters by comparing the modeled and observed WTD (Table 1). To reduce the influence of WTD prediction error on soil thermal and biogeochemical processes, the observed WTDs were used during the simulations if the measurements were available, and the simulated WTDs from this calibrated model were used to interpolate daily values between observations. WTD observations at the sphagnum and eriophorum sites were made on about one-third of the days across seven growing seasons from 2003 to 2009. For the palsa site, we assumed that there

Table 1. The hydrological parameters used for modeling lateral flows*.

Sites	SIR	SOD (m)	SOR	GOD (m)	GOR
Sphagnum	1.0	0	1.0	0.25	0.01
Eriophorum	2.0	−0.05	0.3	0.05	0.01

* SIR, surface inflow rate, the fraction ($m\,m^{-1}$) of rainfall (or water from snow melt) flowing into the site from its surroundings; SOD, surface outflow depth, the water table (WT) depth (positive for below ground and negative for above ground) above which surface lateral outflow occurs; SOR, surface outflow rate, the fraction ($m\,m^{-1}$) of water above the SOD which will be lost as surface outflow per day; GOD, ground outflow depth, the deepest WT depth above which ground outflow occurs; GOR, ground outflow rate, the fraction ($m\,m^{-1}$) of water above the GOD which will be lost as ground outflow per day. These hydrological parameters were determined by calibrating against data sets of water table depth.

is no surface lateral inflow and water will flow away each day when the water table is above the land surface or water infiltrates into frost table, based on local studies (Rydeń et al., 1980). DNDC also requires phenological and physiological parameters to simulate plant growth, including maximum biomass production and its partitioning to shoot and root, vegetation C / N ratio, required thermal degree days for vegetation growth, plant water requirement, and an index of biological N fixation. These parameters for the three land cover types were determined either based on the literature or as model defaults (Table 2).

To initialize the soil climate conditions, the soil thermal and hydrological modules of DNDC were iteratively run by using the climate data in 2002 until the simulated annual mean soil temperature was stable. Then the vegetation and soil biogeochemical modules were activated and the model was run continuously from 2002 to 2009. (Note that soil initial conditions have only a small influence on DNDC output as compared to other factors; therefore, although we did not turn on the vegetation and soil biogeochemical modules during the initialization of soil climate conditions, potential errors in soil initial conditions due to this were small.) We validated the model by using the measured soil thaw depth, NEE, and CH_4 fluxes; using the sign convention that positive values represent net CO_2 or CH_4 emissions into the atmosphere and negative fluxes represent net CO_2 or CH_4 uptake. Two statistical indexes, the relative root-mean-squared error (RRMSE, Eq. 1) and the correlation coefficient (R, equation 2), were used to quantity the accordance and correlation between model predictions and field observations (Moriasi et al., 2007).

$$\mathrm{RRMSE} = \frac{100}{\overline{|o|}}\sqrt{\frac{\sum_{i=1}^{n}(p_i - o_i)^2}{n}}, \quad (1)$$

$$R = \frac{\sum_{i=1}^{n}(o_i - \overline{o})(p_i - \overline{p})}{\sqrt{\sum_{i=1}^{n}(o_i - \overline{o})^2 \sum_{i=1}^{n}(p_i - \overline{p})^2}}. \quad (2)$$

In both equations, o_i and p_i are the observed and simulated values, respectively; $\overline{o}$ and $\overline{p}$ are their averages; and n is the number of values. In addition, we decomposed the root-mean-squared error into systematic and unsystematic components by using the ordinary least-squares (OLS) method (Willmott, 1982; Willmott et al., 1985). The systematic and unsystematic root-mean-squared errors ($\mathrm{RMSE_S}$ and $\mathrm{RMSE_U}$) were calculated using Eqs. (3) and (4), respectively:

$$\mathrm{RMSE_S} = \sqrt{\frac{\sum_{i=1}^{n}(\widehat{p_i} - o_i)^2}{n}}, \quad (3)$$

$$\mathrm{RMSE_U} = \sqrt{\frac{\sum_{i=1}^{n}(p_i - \widehat{p_i})^2}{n}}. \quad (4)$$

In both equations, $\widehat{p_i}$ is an OLS estimate of p_i and is derived from the regression of p_i on o_i by using the ordinary least-squares method (Willmott, 1982; Willmott et al., 1985).

To quantify the differences of C fluxes for the three land cover types across the permafrost thaw gradient, we analyzed the simulated annual NEE and CH_4 fluxes from 2003 to 2009. The CH_4 fluxes from dry palsa were assumed to be zero (Bäckstrand et al., 2008). We calculated net emissions of greenhouse gases (GHG) for the three land cover types as CO_2 equivalents by using a 100-year global warming potential (GWP) of 25 kg CO_2-eq. kg^{-1} CH_4 (IPCC, 2007). In addition, we estimated the possible impacts of permafrost thaw on C fluxes and GHG emissions for the Stordalen mire based on the model results and changes in the fractions of the three land cover types from 1970 to 2000.

3 Results and analyses

3.1 Model validation

3.1.1 Thaw depth

Figure 2 shows the seasonal dynamics of the observed and simulated thaw depth from 2003 to 2009. As field observations demonstrate, thaw rates varied across the three land cover types. At the palsa site, the maximum thaw depth usually ranged from 45 to 60 cm during the summer seasons from 2003 to 2009, while the soil was often thawed to greater than 90 cm (i.e., below the maximum depth of observations) by August or September at the sphagnum site and by June or July at the eriophorum sites. Therefore, the thaw rates were relatively slow, moderate, and rapid at the palsa, sphagnum, and eriophorum sites, respectively. In comparison with the observations, the DNDC model generally captured the differences of thaw depth across the three land cover types as well as their seasonal dynamics (Fig. 2). The simulations showed that the dry palsa site had an active layer thickness of around 55 cm. The thaw depth reached deeper than 100 cm by the end of July to September at the semiwet sphagnum site and by June or July at the wet eriophorum site.

Table 2. The physiological parameters used for simulating plant growth.

Sites	MP[a]	SRF[b]	C / N[c]	TDD[d]	WR[e]	Vascularity	NFI[f]
Palsa	1000	0.35/0.65	90	1500	100	0	1.0
Sphagnum	1200	0.7/0.3	90	1500	100	0	1.1
Eriophorum	2500	0.5/0.5	90	1500	100	1	1.5

[a] MP, the maximum productivity under optimum growing conditions (kg C ha^{-1}). The values were estimated from Rosswall et al. (1975), Malmer and Walleń (1996), and Malmer et al. (2005).
[b] SRF, the shoot and root fractions. The values were estimated from Ström and Christensen (2007) and Olsrud and Christensen (2011). Note that the vegetation at the sphagnum site is not 100 % moss.
[c] C / N, carbon-to-nitrogen ratio of the plant biomass. The values were estimated from Aerts et al. (1992, 2001).
[d] TDD, the required accumulated air temperature heat sum above a 0 °C threshold during the growing season (unit: °C •day) for full vegetation growth.
[e] WR, amount of water required by the plant (g water g^{-1} dry matter).
[f] NFI, index of biological nitrogen fixation.

The model results demonstrated that rate of summer thaw accelerated along the gradient of soil moisture. At the palsa site, the modeled maximum thaw depth ranged between 50 and 60 cm during the summer seasons from 2003 to 2009, while the soil was often thawed to greater than 90 cm by August at the sphagnum site and by June or July at the eriophorum sites. Because water-filled pores have higher thermal conductivity than air-filled pores, DNDC simulated the low, moderate, and high values of thermal conductivity at the dry palsa, semiwet sphagnum, and wet eriophorum sites, respectively, which consequently resulted in the slow, moderate, and fast rates of summer thaw at these three sites. This explanation is consistent with the conclusion based on the local field study (Rydén and Kostov, 1980). However, a few discrepancies remained between the modeled and observed results, primarily in the soil thaw dynamics at the sphagnum site, where DNDC overestimated the thaw rate during the late periods of soil thaw in most years (Fig. 2h–n). Nevertheless, the comparisons between the simulations and observations indicated that DNDC can reliably predict differences in the dynamics of soil thaw at the three land cover types at Stordalen, which is crucial for correctly simulating the impacts of permafrost thaw on soil hydrology, plant growth, and biogeochemical processes.

3.1.2 NEE

Figure 3a–g illustrate the observed and simulated daily NEE at the palsa site. The daily observations were highly variable and showed a clear seasonal cycle across 2003 to 2009, with net CO_2 uptake increasing in early summer, CO_2 uptake most days during mid-summer and net CO_2 emissions in late summer and in autumn. In comparison with the measurements, DNDC generally captured the magnitude and seasonal characteristics of daily NEE, although discrepancies existed. The R values were calculated for each year and ranged from 0.40 to 0.69 (Fig. 3a–g), indicating that there were significant correlations between the simulated and observed daily NEE in each year ($P < 0.0001$). Table 3 lists the observations and simulations on the cumulative NEE for the seven growing periods from 2003 to 2009. The observed cumulative NEE ranged from -435 to -241 kg CO_2-C ha^{-1} and the modeled values ranged from -414 to -265 kg CO_2-C ha^{-1}. The calculated RRMSE values varied between 3 and 25 % (mean: 13%) across the seven growing seasons and the discrepancies between the simulations and observations were less than the standard deviations of the observed cumulative NEE in each year (Table 3). These results indicate that DNDC successfully simulated the cumulative NEE during growing seasons.

At the sphagnum site, the simulated and observed seasonal variations of daily NEE were similar across 2004 to 2009. Both the simulations and observations showed that net CO_2 uptake increased in early summer, prevailed most days during mid-summer, and decreased to net CO_2 emissions in late summer and in autumn (Fig. 3i–n). The similar patterns suggest that the DNDC model generally captured the seasonal fluctuations of daily NEE over 2004 to 2009, although discrepancies existed in each year. However, it seems systematic biases appeared in 2003. For example, the field observations showed high net uptake rates of CO_2 from 25 May to 22 June in 2003, while the model predicted lower rates (Fig. 3h), primarily because of limitations of low solar radiation, air temperature (the mean was 6.0 °C between 25 May and 22 June), and soil temperature on plant productivity. Nonetheless, the modeled and observed daily NEE were significantly correlated in all years ($P < 0.001$ in 2003 and $P < 0.0001$ in other years), and R values ranged from 0.32 to 0.78 (Fig. 3h–n). The predicted cumulative NEE ranged from -521 to -203 kg CO_2-C ha^{-1} over seven growing seasons. The results are consistent with the corresponding observations, which ranged from -525 to -212 kg CO_2-C ha^{-1} (Table 3), with the discrepancies between the simulations and observations close to or less than the standard deviations of the observed cumulative NEE in each year. The values of RRMSE ranged from 1 to 17 %, with a mean of 6 % over 2003 to 2009 (Table 3).

At the eriophorum site, both the simulated and observed daily NEE showed similar seasonal patterns across the studied years, except for 2004 (Fig. 3o–u), with net CO_2 uptake

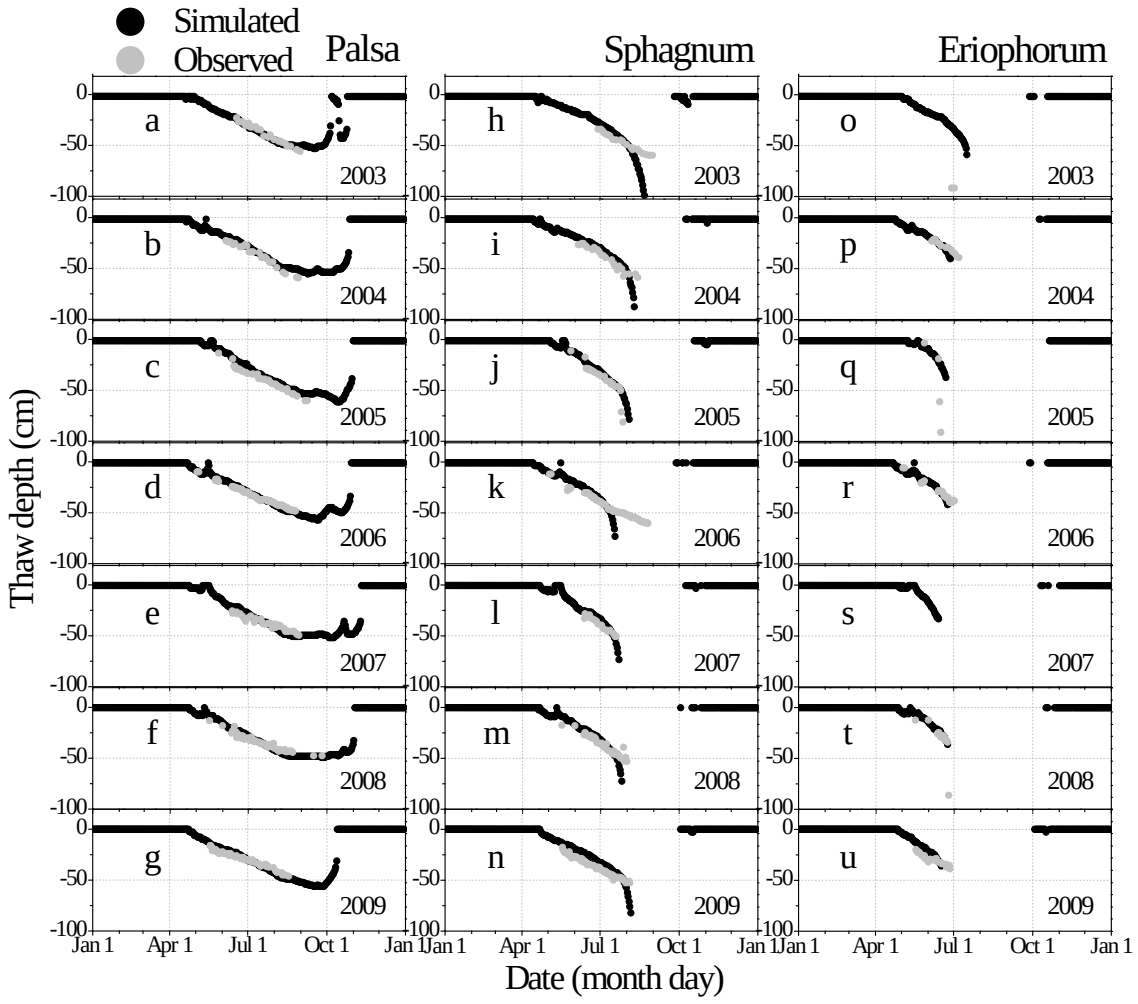

Figure 2. Simulated and observed seasonal dynamics of thaw depth at the palsa **(a–g)**, sphagnum **(h–n)**, and eriophorum **(o–u)** sites from 2003 to 2009. The entire soil layer was thawed at the beginning of field observations (in mid-June) at the eriophorum site in 2007 **(s)**.

increasing in early summer, CO_2 uptake most days during mid-summer and net CO_2 emissions in late summer and in autumn. The R values ranged from 0.39 to 0.74, which indicates significant ($P < 0.0001$) correlations between the modeled and measured daily NEE in each year from 2003 to 2009. However, we also note systematic deviation between the simulations and measurements in 2004. In this year, the field observations showed persistent low net uptake rates of CO_2 during the period of late May to the end of June, while the model predicted an increasing trend of net CO_2 uptake (Fig. 3p), because of increasing solar radiation, air temperature, soil temperature, and soil thaw depth. At the eriophorum site, the observed daily uptake rates of CO_2 were usually higher than that at the palsa and sphagnum sites during summer (Fig. 3). The DNDC model captured the differences across these three sites, and the magnitudes of the simulated NEE were comparable with the corresponding observations. The simulations of growing season cumulative NEE ranged from -1078 to $-365\,\mathrm{kg\,CO_2\text{-}C\,ha^{-1}}$ from 2003 to 2009, which were close to the observations (ranging from -1118 to $-270\,\mathrm{kg\,CO_2\text{-}C\,ha^{-1}}$). The RRMSE values ranged from 1 to 35 % (mean: 15 %) over the period 2003 to 2009 (Table 3). The discrepancies between the simulated and observed cumulative NEE were less than the standard deviations of the observations in each year from 2003 to 2007, which indicates DNDC reliably simulated the growing season cumulative NEE over these years. However, the discrepancies were larger than the standard deviations of the observed cumulative NEE in 2008 and 2009 (-571 vs. $-471 \pm 76\,\mathrm{kg\,C\,ha^{-1}}$ in 2008, and -365 vs. $-270 \pm 59\,\mathrm{kg\,C\,ha^{-1}}$ in 2009), suggesting that the model may have overestimated the CO_2 uptake during the growing season in these 2 years.

3.1.3 Water table and CH_4 fluxes

As shown in Fig. 4a–g, WTDs (with positive values for above ground and negative values for below ground) fluctuated

Table 3. Comparison of the modeled (M) and observed (O) net ecosystem exchanges (NEE, in kg C ha^{-1}) of CO_2 during growing periods at the palsa, sphagnum, and eriophorum sites[a].

Year	Palsa			Sphagnum			Eriophorum		
	O[b]	M	RRMSE[c]	O	M	RRMSE	O	M	RRMSE
2003	−330[264]	−414	25	−394[59]	−326	17	−1118[219]	−1078	4
2004	−241[269]	−265	10	−441[73]	−452	2	−815[449]	−870	7
2005	−338[369]	−347	3	−525[69]	−521	1	−741[450]	−980	32
2006	−386[283]	−319	17	−356[27]	−330	8	−1034[94]	−1019	1
2007	−338[187]	−353	4	−436[114]	−424	3	−930[208]	−980	5
2008	−399[263]	−328	18	−264[79]	−288	9	−471[76]	−571	21
2009	−435[129]	−380	13	−212[75]	−203	4	−270[59]	−365	35

[a] The growing period in this study is defined as the periods during which measurements of continuous net CO_2 uptake were available. To calculate the total NEE over the growing period in each year, fluxes for the days lacking measurements were determined using the arithmetic mean fluxes of the two closest days when observations were performed. Daily fluxes from either direct measurements or gap filling were then summed up to calculate the growing period cumulative NEE.
[b] Each figure number within brackets is the standard deviation of three (palsa and sphagnum) or two (eriophorum) replicate autochamber plots.
[c] RRMSE, relative root-mean-squared error, %.

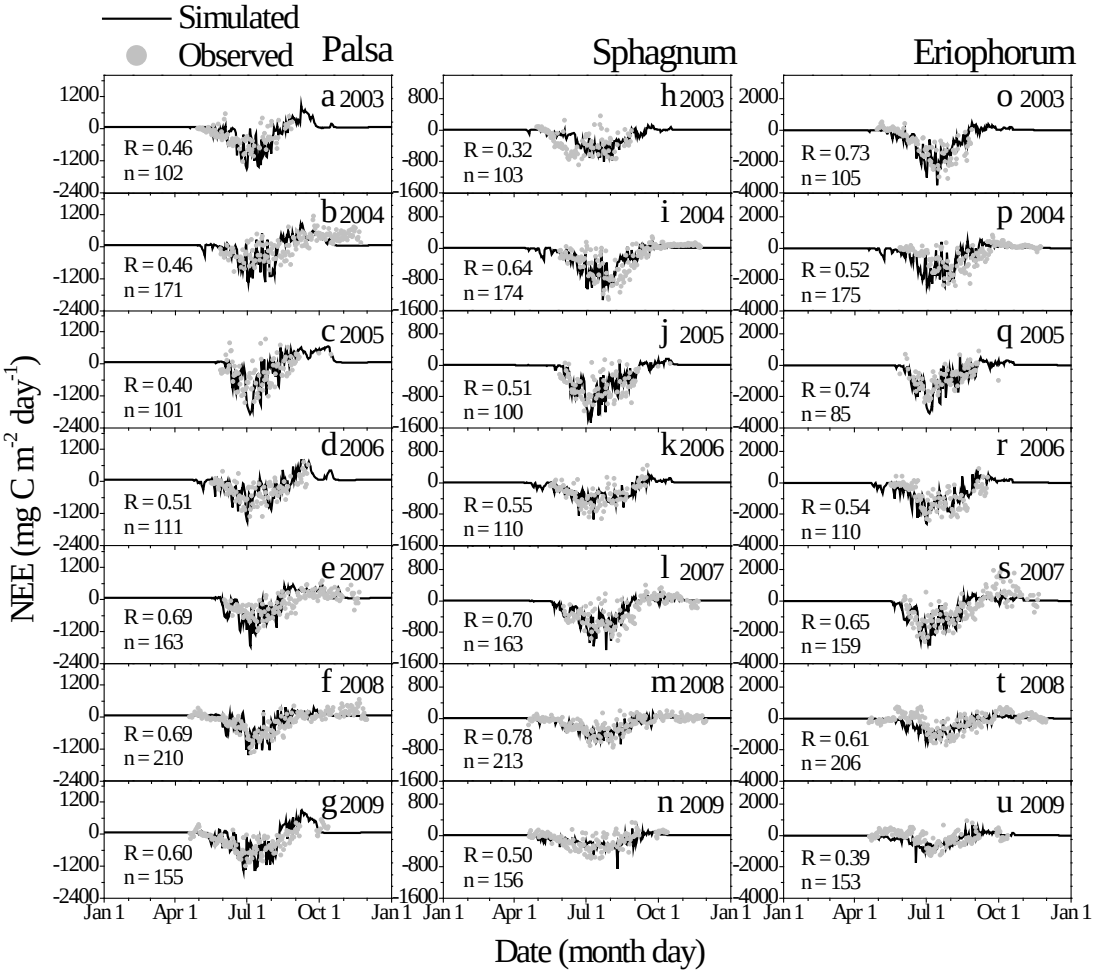

Figure 3. Simulated and observed daily net ecosystem exchange (NEE) of CO_2 (mg C m^{-2} day^{-1}) at the palsa **(a–g)**, sphagnum **(h–n)**, and eriophorum **(o–u)** sites from 2003 to 2009. The correlations between the simulated and observed daily NEE were significant for all cases ($P < 0.0001$, except for **(i)**, where $P < 0.001$). The observed data are the means of three (palsa and sphagnum) or two (eriophorum) chamber replicates and, for reasons of clarity, standard deviations are not shown. Note that the vertical axis scales for NEE are different across the three sites.

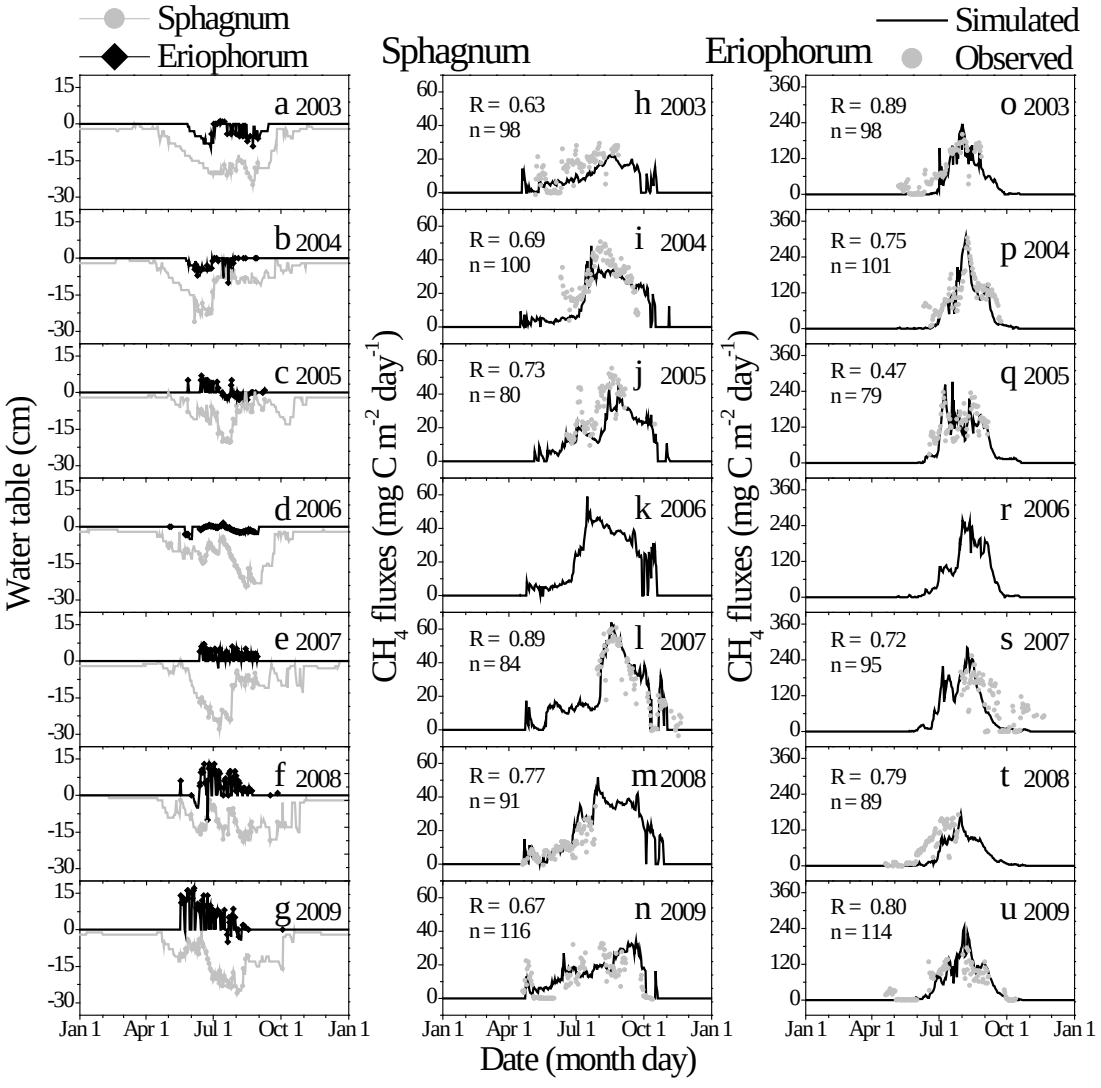

Figure 4. Simulated (lines) and observed (dots) water table dynamics **(a–g)**, daily CH_4 fluxes (mg C m^{-2} day^{-1}) at the sphagnum **(h–n)** and eriophorum **(o–u)** sites from 2003 to 2009. The correlations between the simulated and observed daily CH_4 fluxes were significant for all cases ($P < 0.0001$). The observed CH_4 fluxes are the means of three (sphagnum) or two (eriophorum) chamber replicates and standard deviations are not shown for reasons of clarity. Because of instrument problems (Bäckstrand et al., 2008), observed data were not used for model evaluation in 2006. Note that the water table depths at both the sphagnum and eriophorum sites are shown in the panels **(a–g)** and the vertical axis scales for CH_4 fluxes are different between the two sites.

between −30 and 0 cm at the sphagnum site, while were generally near or above the ground surface at the eriophorum site.

Figure 4h–n compare the observed and simulated daily CH_4 fluxes at the sphagnum site. As illustrated by Fig. 4h–n, the simulated seasonal patterns of daily CH_4 fluxes were close to the observations during the six studied years from 2003 to 2009 (excluding 2006, which had no data), with the highest peak appeared in August or September in both the simulations and field measurements. In addition, DNDC simulated small spikes of CH_4 emission a few days after snowmelt and during the post-growing season, which also agreed with the observations (Fig. 4l–n). The simulated early CH_4 flux spikes were induced by snowmelt and thaw of surface soil layer, which created water saturation in surface peat and thereby supported CH_4 production and emission. The high fluxes predicted during the post-growing season occurred during occasional thaw of the surface soil layer during the early freezing stage, which provided pathways of releasing for both newly produced methane and methane accumulated in the soil profile. The R values ranged between 0.63 and 0.89 over the 6 years (Fig. 4h–n), which indicates the simulated seasonal variation of daily CH_4 fluxes was significantly correlated with the observed seasonal variation in

each year ($P < 0.0001$). The similar patterns and significant correlations between the simulated and observed daily CH_4 fluxes suggest that DNDC generally captured the observed seasonal characteristics of CH_4 fluxes, despite a few remaining inconsistencies. The modeled results indicated that the temporal patterns of CH_4 fluxes were primarily controlled by soil temperature and the changes of WTD at the sphagnum site. Simulated daily CH_4 fluxes were positively correlated with soil temperature ($P < 0.0001$) when WTDs were closer to the peat surface than -10 cm (Fig. 5a). Simulated daily CH_4 fluxes were also positively correlated with the WTDs ($P < 0.0001$) if the mean of peat layer (0–50 cm) temperature was higher than 2.0 °C (Fig. 5b). Of the six tested sampling periods, the simulated cumulative CH_4 fluxes varied from 12.7 to 35.7 kg CH_4-C ha^{-1}, comparable with the observations, which varied from 9.7 to 30.6 kg CH_4-C ha^{-1} (Table 4). The values of RRMSE ranged from 4 to 35 %, with a mean of 21 % (Table 4). The comparison demonstrates that the discrepancies between the simulated and observed cumulative CH_4 fluxes were close to or less than the standard deviations of the observations in each year.

At the eriophorum site, the observed CH_4 fluxes usually started to increase early in the growing season, with high peaks appearing between July and September. Then the CH_4 fluxes decreased during the rest of growing season (Fig. 4o–u). The simulated seasonal patterns of daily CH_4 fluxes were comparable with the observations, with a generally increasing trend from the early growing season until mid-summer in each year, when the fluxes reached relatively high levels. Then the simulated CH_4 fluxes started to decrease (Fig. 4o–u). The correlations between the modeled and measured daily CH_4 fluxes were statistically significant ($P < 0.0001$) in each year, with R values ranging from 0.47 to 0.89 over the 6 years. These results suggest that DNDC approximately matched the observed daily CH_4 fluxes over the six studied years from 2003 to 2009 (excluding 2006), although discrepancies existed in each year. However, it seems systematic biases existed in 2008. DNDC underestimated the magnitudes of CH_4 fluxes in 2008 and had a relatively later onset of emissions than observations (Fig. 4t). The modeled results demonstrated that the temporal patterns of CH_4 fluxes at the eriophorum site were mainly related to the changes in soil temperature and the associated variations of plant growth and soil decomposition, because of the inundated conditions at this site, which generated constantly wet anaerobic conditions suitable for CH_4 production. Simulated daily CH_4 fluxes were positively correlated with soil temperature (Fig. 5c, $P < 0.0001$), and we did not find any correlation between the simulations of daily CH_4 fluxes and WTD (Fig. 5d). This conclusion is consistent with the field results (e.g., Bäckstrand et al., 2008; Jackowicz-Korczyński et al., 2010). As illustrated by Fig. 4h–u, the observed daily CH_4 fluxes at the eriophorum site were generally higher than that at the sphagnum site. DNDC captured the differences between these two sites. Of the six tested sampling periods, the observed cumulative CH_4 fluxes ranged from 57.9 to 121 kg CH_4-C ha^{-1}, while the modeled results varied from 45.5 to 113 kg CH_4-C ha^{-1}. The RRMSE values ranged from 3 to 22 %, with a mean of 12 % across these six periods (Table 4). The discrepancies between the simulations and observations were close to or less than the standard deviations of the observed cumulative CH_4 fluxes over the studied years except for 2003 and 2008, which indicates a good accordance between the simulations and observations of CH_4 fluxes over these years. However, the discrepancy was larger than the standard deviation of the observed cumulative CH_4 fluxes in 2003 and 2008 (76.4 vs. 91.8 ± 10.5 kg C ha^{-1} in 2003, and 45.3 vs. 57.9 ± 4.42 kg C ha^{-1} in 2008), suggesting that the model may have underestimated the cumulative CH_4 fluxes in these 2 years.

3.2 Annual C fluxes and net greenhouse gas emissions

In this section, we review simulated annual (not growing season) NEE and CH_4 fluxes at the palsa, sphagnum, and eriophorum sites from 2003 to 2009. The simulated annual total NEE varied from -132 to $+56.5$ (palsa; mean: -50.9), -492 to -191 (sphagnum; mean: -342), and -1021 to -399 (eriophorum; mean: -793) kg CO_2-C ha^{-1} yr^{-1}, and interannual variability of NEE increased with increasing magnitude (Fig. 6a). The predictions of annual total NEE were different across the palsa, sphagnum, and eriophorum sites and primarily resulted from differences in environmental conditions, including soil temperature, thaw regime (Fig. 2), soil moisture content (Fig. 4a–g), and vegetation characteristics (as indicated by the different physiological parameters used for simulating plant growth, Table 2). DNDC predicted the highest uptake rates of CO_2 at the eriophorum site, primarily due to (1) the highest value of the maximum productivity under optimum growing conditions (Table 2); (2) the fastest soil thaw rate (Fig. 2), which was favorable for water and nitrogen uptake; and (3) a permanently high water table (Fig. 4a–g), which restricted soil heterotrophic respiration and provided abundant water for plant transpiration. The lowest rates of annual total NEE were simulated at the palsa site, primarily because of (1) the lowest value of the maximum productivity under optimum growing conditions (Table 2), (2) the slowest soil thaw rate and limited summer thaw depths (Fig. 2), and (3) a relatively dry soil which restricted plant transpiration and was comparatively favorable for soil decomposition.

From 2003 to 2009, the simulations of annual total CH_4 fluxes ranged from 17.9 to 42.2 (sphagnum; mean: 32.8) and 72.2 to 125 (eriophorum; mean: 104) kg CH_4-C ha^{-1} yr^{-1}. As with NEE simulations, interannual variability of CH_4 fluxes increased with increasing annual means (Fig. 6a). The annual total CH_4 fluxes were different across the sphagnum and eriophorum sites (Fig. 6a). Simulated CH_4 fluxes were higher at the eriophorum site than the sphagnum site due to (1) increased rates of CH_4 production due to higher soil

Table 4. Comparison of the modeled (M) and observed (O) CH_4 fluxes (in kg C ha^{-1}) during six study periods at the sphagnum and eriophorum sites[a].

Year	Sphagnum			Eriophorum		
	O[b]	M	RRMSE[c]	O	M	RRMSE
2003	17.2[5.2]	12.2	29	91.8[10.5]	76.4	17
2004	30.6[8.0]	24.3	21	121[14.7]	105	13
2005	25.1[4.7]	24.1	4	108[60.6]	101	7
2007	30.4[7.5]	35.7	18	116[22.2]	113	3
2008	9.7[4.2]	13.1	35	57.9[4.42]	45.3	22
2009	23.2[7.5]	27.5	18	111[21.7]	101	9

[a] The study period is the span during which continuous measurements of daily CH_4 fluxes were available. To calculate the total CH_4 emissions over the sampling period in each year, fluxes for the days lacking measurements were determined using the arithmetic mean fluxes of the two closest days when observations were performed. Daily fluxes from either direct measurements or gap filling were then summed up to calculate the cumulative CH_4 emissions over the sampling period.
[b] Each figure number within brackets is the standard deviation of three (sphagnum) or two (eriophorum) replicate autochamber plots.
[c] RRMSE, relative root-mean-squared error, %.

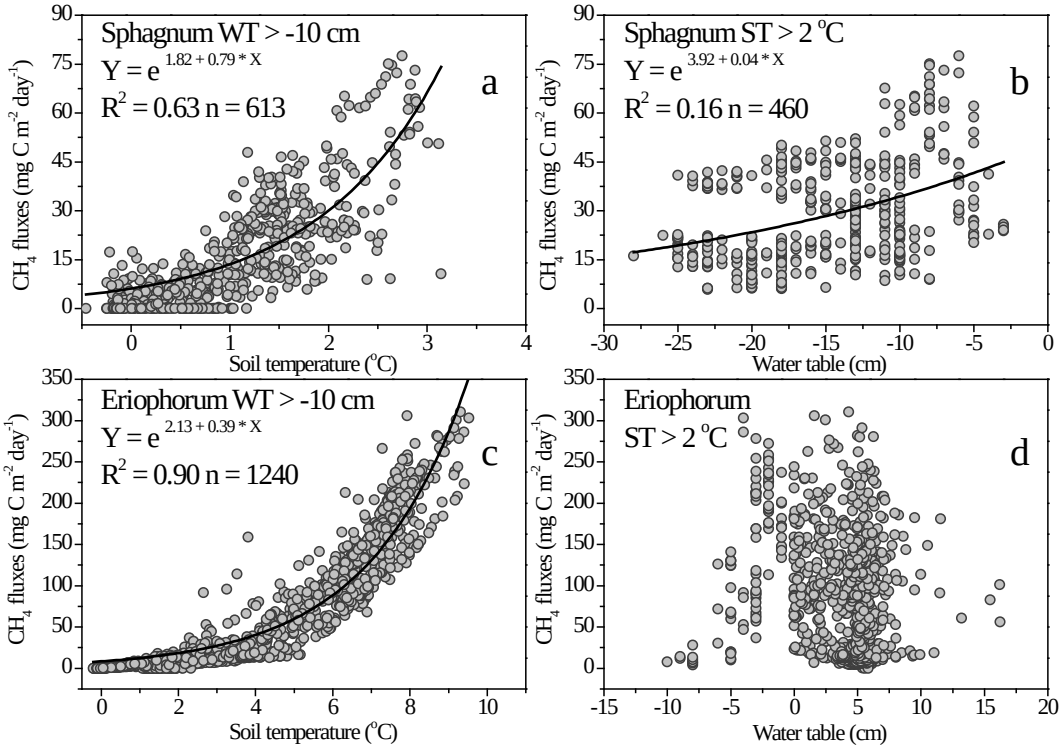

Figure 5. Relationships between simulated CH_4 fluxes and average soil (0–50 cm) temperatures, as well as water table depths at the sphagnum **(a–b)** and eriophorum **(c–d)** sites. The results shown in **(a)** and **(c)** are for periods with water table depth above −10 cm; the results shown in **(b)** and **(d)** are for periods with average soil temperature (ST, 0–50 cm) > 2 °C. The relationships shown in **(a)**, **(b)**, and **(c)** were significant ($P < 0.0001$).

temperature and faster thaw rate, (2) a higher water table that supported CH_4 production while restricting CH_4 oxidation, (3) higher plant growth rates and consequently more substrates (e.g., CO_2 and dissolved organic carbon) used for CH_4 production, and (4) accelerated rates of CH_4 transport due to increased plant vascularity.

Annual net C fluxes were calculated as the sum of annual total NEE and CH_4 fluxes in this study (i.e., horizontal loss of dissolved organic carbon was not considered). Because the CH_4 component was assumed to be zero at the palsa site, the simulated annual net C fluxes were equal to annual NEE (range: −132 to 56.5 kg C ha^{-1}; mean: −50.9 kg C ha^{-1}) at

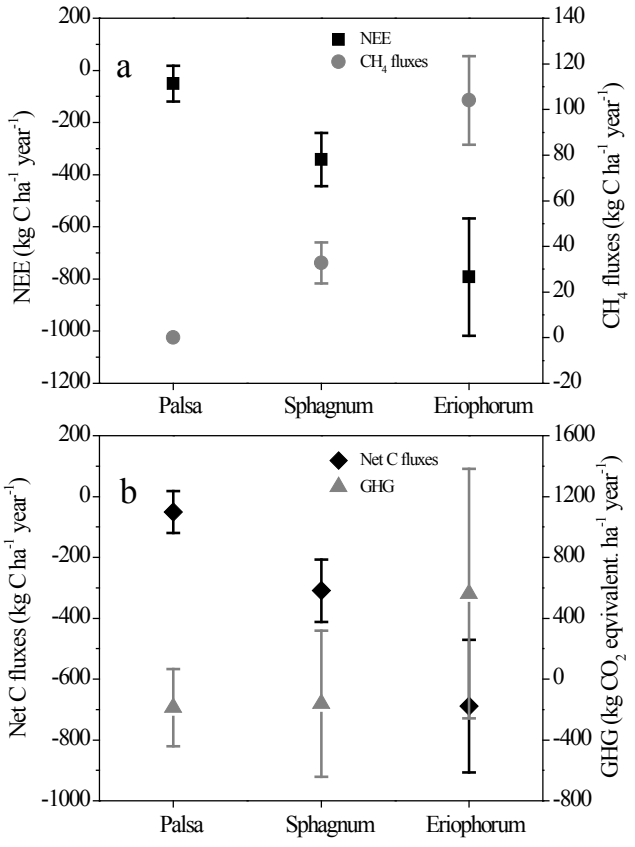

Figure 6. Simulated net ecosystem exchange (NEE) of CO_2, CH_4 fluxes, net carbon fluxes, and net emissions of greenhouse gases (GHG) at the palsa, sphagnum, and eriophorum sites. The CH_4 fluxes from the dry palsa site were assumed negligible (here 0), based on field observations. Data are means of annual total fluxes from 2003 to 2009. Vertical bars are standard deviations of annual total fluxes from 2003 to 2009 and indicate interannual variations of C gas fluxes.

this site. Simulations of annual net C fluxes ranged between −462 and −163 (mean: −309) and between −934 and −488 (mean: −689) kg C ha^{-1} at the sphagnum and eriophorum sites, respectively, from 2003 to 2009. These results illustrated that C uptake rates increased along the permafrost thaw gradient at Stordalen (Fig. 6b). Net GHG emissions, expressed as CO_2 equivalents, were calculated by considering more powerful radiative forcing potential of CH_4 than CO_2 (25 times over a 100-year horizon). The simulated annual GHG at the palsa site varied from −485 to 207 kg CO_2-eq. ha^{-1} yr^{-1}, with a mean of −186 kg CO_2-eq. ha^{-1} yr^{-1} from 2003 to 2009. At the sphagnum and eriophorum sites, the annual GHG ranged from −806 to 377 and −849 to 1905 kg CO_2-eq. ha^{-1} yr^{-1}, respectively, and the corresponding means were −162 and 562 kg CO_2-eq. ha^{-1} yr^{-1}, respectively. Therefore, the modeled results demonstrated that, for the wetter eriophorum site, higher CH_4 emissions offset its larger net C sink, and the palsa site was a larger net sink of CO_2 equivalents than the eriophorum site (Fig. 6b).

3.3 Possible changes of C fluxes due to permafrost thaw at Stordalen

Interpretation of aerial images of Stordalen showed that the area of "hummock" (palsa) cover declined from 9.2 to 8.3 ha, while the area of "semiwet" and "wet" (sphagnum) cover increased from 6.0 to 6.2 ha, and "tall graminoid" (eriophorum) cover increased from 1.3 to 2.0 ha from 1970 to 2000 (Malmer et al., 2005; T. Johansson et al., 2006). These changes in vegetation cover indicate a trend toward a wetter ecosystem probably as a direct consequence of permafrost thaw at Stordalen. Given that soil thaw rate accelerated under wet conditions (Fig. 2), this trend toward a wetter ecosystem (i.e., from palsa into sphagnum or eriophorum) may further accelerate permafrost degradation. By applying the modeled annual CO_2 and CH_4 fluxes to these changes in vegetation cover areas, we estimated an increase of 578 kg C yr^{-1} (or 35 kg C ha^{-1} yr^{-1} for the study area of 16.5 ha) in CO_2 uptake and an increase of 79 kg C yr^{-1} (or 4.8 kg C ha^{-1} yr^{-1}) in CH_4 emission from 1970 to 2000 at Stordalen. Using a 100-year GWP value for methane, the net impact due to the vegetation change is a net CO_2-equivalent emission of 527 kg CO_2-eq. yr^{-1}; in other words, the warming impact of increased CH_4 emission more than offsets the cooling impact of increased CO_2 uptake at the mire. If these fluxes from vegetation cover areas (1970 vs. 2000) were to persist for one to two centuries, an analysis with a simple model of atmospheric perturbation radiative forcing (Frolking et al., 2006) shows that the different atmospheric lifetimes of CO_2 and CH_4 are such that the CO_2 sink would overcome the CH_4 emissions in terms of instantaneous radiative forcing and the climate impact of this vegetation change would eventually switch to a net cooling after about 120 years. Note that the simulated C fluxes over winter are not well constrained by field data at this time.

4 Discussion

4.1 Validation of DNDC

In this study, we applied the new version of DNDC to simulate soil freeze–thaw dynamics and C fluxes across three typical land cover types (i.e., palsa, sphagnum, and eriophorum) at Stordalen, Sweden, which are considered to represent a gradient of permafrost thaw (T. Johansson et al., 2006; Bäckstrand et al., 2010). Both field observations and DNDC simulations showed significant differences in C fluxes across these three land cover types and the simulated rates of seasonal cumulative C fluxes were comparable with the corresponding measurements for most cases (Tables 3 and 4). These results indicate that the model successfully captured the differences in C fluxes among these land cover types. In addition, the

model generally captured the magnitudes and temporal dynamics of soil thaw, NEE, and CH_4 fluxes (Figs. 2, 3, and 4). The model validation suggests that the enhanced DNDC can potentially be used to predict impacts of permafrost thaw, but cannot yet independently simulate subsequent changes in soil hydrology and vegetation, which influence C dynamics in northern peatlands. We also note some discrepancies between the modeled results and the field measurements.

Compared to daily observations of NEE, DNDC overestimated CO_2 uptake rates (i.e., predicted more negative NEE) on a few days during the growing seasons (Fig. 3), which may have resulted from over-prediction of photosynthesis, causing DNDC to predict higher NPP. Because meteorological data at the ANS (10 km northwest of Stordalen) were used to support the simulations and photosynthesis is closely related to climate factors, deviations in predicting daily variability in photosynthesis may be caused by lacking site-specific data. Local observations also demonstrated that meteorological conditions were different between Stordalen and ANS (Olefeldt and Roulet, 2012; Rydén, 1980). These differences inevitably affected model simulations of C fluxes. We further calculated the $RMSE_S$ and $RMSE_U$ for daily NEE (Table 5). The results demonstrate that systematic errors accounted for 11, 25, and 23 % of the mean-square errors in daily NEE at the palsa, sphagnum, and eriophorum sites, respectively. Therefore the discrepancies between the modeled and measured NEE could be primarily attributed to random components, including absence of site-specific data. However, we also note systematic discrepancies between the modeled and observed NEE at both the sphagnum and eriophorum sites. Inconsistent with field data in other years, high net uptake rates of CO_2 occurred at the sphagnum site during the period of 25 May to 22 June in 2003 (Fig. 3h–n), even though solar radiation, air temperature, and soil temperature were low (Fig. 1) and soil thaw depth was shallow (Fig. 2h), causing DNDC to predict lower uptake rates. At the eriophorum site, the model predicted an increasing trend of net CO_2 uptake (Fig. 3p) from late May to the end of June in 2004 because of the increases in solar radiation, air temperature, and soil thaw depth, while the field observations showed persistent low net CO_2 uptake rates. Further studies are needed to clarify the differences in seasonal characteristics of NEE between 2003 and other years at the sphagnum site, as well as the inconsistencies between the predictions and observations.

DNDC approximately matched the observed daily CH_4 fluxes at both the sphagnum and eriophorum sites (Fig. 4). However, we also note a few inconsistencies between the simulations and observations (e.g., in 2003 at the sphagnum site and in 2008 at the eriophorum site). Model parameters for soil and vegetation characteristics were derived from a number of studies done at Stordalen since the International Biosphere Program in the early 1970s (Sonesson et al., 1980). Because these parameters have strong influences on soil climate, plant growth, and soil biogeochemistry

Table 5. The systematic and unsystematic root-mean-squared errors ($RMSE_S$ and $RMSE_U$) between the modeled and observed daily net ecosystem exchanges (NEE) of CO_2 and CH_4 fluxes at the palsa, sphagnum, and eriophorum sites.

Sites	NEE ($mg\,C\,m^{-2}\,day^{-1}$)		CH_4 fluxes ($mg\,C\,m^{-2}\,day^{-1}$)	
	$RMSE_S$	$RMSE_U$	$RMSE_S$	$RMSE_U$
Palsa	140	405		
Sphagnum	119	206	4.7	8.4
Eriophorum	298	545	16.7	46.6

in DNDC, potential biases in inputs could affect model results, including CH_4 fluxes. The calculations of $RMSE_S$ and $RMSE_U$ (Table 5) also demonstrate that most of the mean-square errors in daily CH_4 fluxes were attributable to random errors, including deviations resulting from biases in model inputs, at both the sphagnum (76 %) and eriophorum (89 %) sites.

In addition, it should be noted that the modeled C fluxes over winter periods remain uncertain because observations utilized for model validation were primarily available during growing seasons. DNDC simulations demonstrated that C fluxes during non-growing season substantially contributed to annual C fluxes at Stordalen. From 2003 to 2009, the means of accumulated CO_2 emissions over non-growing seasons were 342, 32.8, and 101 $kg\,CO_2\text{-}C\,ha^{-1}$, respectively, at the palsa, sphagnum, and eriophorum sites. Local field studies also indicated that net CO_2 emissions over winter periods significantly contributed to annual NEE at both dry and wet areas (Bäckstrand et al., 2010; Christensen et al., 2012) and accumulation of net CO_2 emissions during winter may have made the dry palsa site a net annual CO_2 source (Bäckstrand et al., 2010). The simulations of average accumulated CH_4 fluxes over non-growing seasons were 9.8 and 13.8 $kg\,CH_4\text{-}C\,ha^{-1}$ at the sphagnum and eriophorum sites, representing 30 and 13 % of mean annual emissions. In the wet area dominated by tall graminoid vegetation, field measurements demonstrated that CH_4 emissions over winter accounted for approximately 19 % of the annually emitted CH_4 (Jackowicz-Korczyński et al., 2010). These results indicate that further tests are necessary to verify the model's predictions of C fluxes during winter periods.

Although the modeled C fluxes were tested against field measurements with encouraging results, we note that uncertainty may exist in simulating individual processes in C transformations. For example, methane flux is predicted by DNDC as the net result of CH_4 production, oxidation, and transport processes. Validating simulations of CH_4 emission against field measurements did not evaluate the DNDC's simulation of these three processes individually. One approach for testing/constraining simulation of the individual processes is to include stable isotopes and isotope fractionation

during the processes of methanogenesis (acetate fermentation and CO_2 reduction), methane oxidation, and methane transport (e.g., Chanton et al., 2005; Corbett et al., 2013). This is planned for future model development.

4.2 Permafrost thaw and C fluxes

Our modeled results provide some indications on how C fluxes will change with ongoing permafrost thaw at Stordalen. If the palsa evolves into sphagnum or eriophorum during permafrost thaw, the mire may be able to sequester more atmospheric C, considering the higher rates of net C uptake shown at the sphagnum or eriophorum sites (Fig. 6b). However, increases of net C uptake were positively correlated with increases of CH_4 emissions across the thaw gradient at Stordalen (Fig. 6), indicating that permafrost thaw will generate a tradeoff of GHG. If the net impact is calculated using the GWP methodology (e.g., Shine et al., 1990), then the balance depends on the relative rate of changes in CO_2 uptake and CH_4 emissions and the time horizon chosen for the GWP calculation (e.g., Frolking and Roulet, 2007; Whiting and Chanton, 2001).

By applying the modeled C fluxes to the areal changes of land cover types at Stordalen, we estimated that the net impact due to the vegetation change is a net CO_2 equivalent emission of $527\,\mathrm{kg\,CO_2\text{-}eq.\,yr^{-1}}$ from 1970 to 2000 at Stordalen. However, it should be noted that this result was calculated by assuming constant annual emissions (equal to the means simulated by DNDC from 2003 to 2009) between 1970 and 2000 and the modeled results showed obvious interannual variability in both NEE and CH_4 fluxes (Fig. 6), and it is not known when during the period of 1970–2000 the land cover change occurred. If the net impact is calculated by considering the interannual variability of C fluxes, the estimation of a net CO_2 equivalent emission from 1970 to 2000 is not significantly ($P = 0.07$) higher than zero. T. Johansson et al. (2006) also used a 100-year GWP value for methane but treated their "wet" cover somewhat differently – equivalent to "semiwet" (sphagnum) for NEE due to similarity in vegetation composition, but with a higher value for CH_4 emission as it was an inundated area. Because the "wet" area was nearly 30 % of the study region and expanded from 1970 to 2000, T. Johansson et al. (2006) estimated that the mire was a GHG source in terms of CO_2 equivalents to the atmosphere, and they reported an increase of 47 % in net radiative forcing from 1970 to 2000 by considering the fluxes during the growing season. Our analysis estimated that the mire was a GHG sink due to a lower value for CH_4 emission in "wet" areas, and yielded an overall decrease of 27 % in net radiative cooling from 1970 to 2000. The differences and uncertainties in these interpretations illustrate an important scaling challenge – how many land cover classes are needed and what are the most important distinctions to consider? This can be evaluated in future analyses by comparison of up-scaling flux by aerial fractions of land cover with multiyear eddy covariance tower fluxes. Flux towers are now operating at Stordalen under the European Integrated Carbon Observation System (ICOS) program (Paris et al., 2012).

4.3 Modeling impacts of permafrost thaw on C fluxes

The modeling of impacts of permafrost thaw on C fluxes is in a very early stage, and much additional work is required for a more complete treatment of all of the processes involved. As shown in this and other studies (e.g., Olefeldt et al., 2013), NEE and CH_4 fluxes are strongly controlled by the soil water regime and vegetation characteristics, which stresses the importance of considering changes in soil hydrology and vegetation when predicting responses of C turnover to climate change in permafrost ecosystems. Although changes in wetland cover and vegetation have been observed along with permafrost degradation in northern peatlands (e.g., Goetz et al., 2011; Smith et al., 2005), most modeling work that predicts impacts of climate change on C turnover is based on static distribution of wetlands and vegetation (Bohn and Lettenmaier, 2010). Therefore biases may result from neglecting changes in the water table regime and vegetation transitions along with permafrost thaw. In this study, we determined different soil water conditions for the three land cover types at Stordalen by combining the observed WTD and the hydrological module of DNDC. The required hydrological parameters were estimated by calibrating against WTD data sets (Table 1). While these parameters were empirically determined, they are consistent with the general topography of Stordalen, with the palsa surface elevated 0.5–2.0 m above the eriophorum surface and the sphagnum surface at intermediate elevation (Olefeldt and Roulet, 2012). However, it should be noted that sufficient WTD data are required for calibrating these hydrological parameters if the model is to be applied to other peatlands. Although different WTD and vegetation characteristics were used as inputs for different land cover types to represent changes in soil water regime and vegetation along with permafrost thaw at Stordalen, it would be ideal to incorporate these changes dynamically into the model's framework for better understanding of how permafrost thaw affect landscape wetness and how this in turn affect vegetation and C fluxes. Our efforts of incorporating a permafrost model should provide a sound approach for the model to incorporate the processes related to changes in soil water regime and vegetation along with permafrost thaw, although important additional processes are needed in a comprehensive biogeochemical model that is fully functional for northern ecosystems.

5 Conclusions

Climate warming and associated permafrost degradation are expected to have significant impacts on the C balance of permafrost ecosystems, but the magnitude is uncertain. We

incorporated a permafrost model, NEST, into a biogeochemical model, DNDC, to model C dynamics in high-latitude ecosystems. The enhanced DNDC model was applied to assess effects of permafrost thaw on C fluxes of a subarctic peatland at Stordalen, Sweden. DNDC simulated soil freeze–thaw dynamics and C fluxes across three typical land cover types (i.e., palsa, sphagnum, and eriophorum) at Stordalen, which span a gradient in the processes of permafrost thaw. Model results were tested against multiyear field measurements. The model validation indicates that DNDC was able to capture differences in seasonal soil thaw, NEE, and CH_4 fluxes across the palsa, sphagnum, and eriophorum sites at Stordalen. In addition, the simulated magnitudes and temporal dynamics of soil thaw, NEE, and CH_4 fluxes were in general agreement with field measurements. Consistent with the results from field studies, the modeled C fluxes across the permafrost thaw gradient demonstrate that permafrost thaw and the associated changes in soil hydrology and vegetation not only increase net uptake of C from atmosphere but also increase the radiative forcing impacts on climate due to increased CH_4 emission. By using the modeled annual C fluxes and reported areas of vegetation cover in 1970 and 2000, we estimated that the Stordalen mire was a net GHG sink (using a 100-year GWP value for methane) and yielded an overall decrease of 27 % in net radiative cooling from 1970 to 2000.

Acknowledgements. This study was supported by the NASA Terrestrial Ecology Program (NNX09AQ36G), the US Department of Energy (DE-SC0004632), and the US National Science Foundation (ARC-1021300). We thank Abisko Scientific Research Station for providing the meteorological data. We thank N. T. Roulet and an anonymous reviewer for comments and suggestions that improved the manuscript.

Edited by: P. Stoy

References

ACIA: Arctic climate impact assessment: scientific report, Cambridge University Press, New York, 2005.

Aerts, R., Wallén, B., and Malmer, N.: Growth-limiting nutrients in *Sphagnum*-dominated bogs subject to low and high atmospheric nitrogen supply, J. Ecol., 80, 131–140, 1992.

Aerts, R., Wallén, B., Malmer, N., and de Caluwe, H.: Nutritional constraints on *Sphagnum*-growth and potential decay in northern peatlands, J. Ecol., 89, 292–299, 2001.

Åkerman, H. J. and Johansson, M.: Thawing permafrost and thicker active layers in sub-arctic Sweden, Permafrost Periglac., 19, 279–292, 2008.

Avis, C. A., Weaver, A. J., and Meissner, K. J.: Reduction in areal extent of high-latitude wetlands in response to permafrost thaw, Nat. Geosci., 4, 444–448, 2011.

Bäckstrand, K., Crill, P. M., Mastepanov, M., Christensen, T. R., and Bastviken, D.: Total hydrocarbon flux dynamics at a subarctic mire in northern Sweden, J. Geophys. Res., 113, G03026, doi:10.1029/2008JG000703, 2008.

Bäckstrand, K., Crill, P. M., Jackowicz-Korczyñski, M., Mastepanov, M., Christensen, T. R., and Bastviken, D.: Annual carbon gas budget for a subarctic peatland, Northern Sweden, Biogeosciences, 7, 95–108, doi:10.5194/bg-7-95-2010, 2010.

Bohn, T. J. and Lettenmaier, D. P.: Systematic biases in large-scale estimates of wetland methane emissions arising from water table formulations, Geophys. Res. Lett., 37, L22401, doi:10.1029/2010GL045450, 2010.

Callaghan, T. V., Bergholm, F., Christensen, T. R., Jonasson, C., Kokfelt, U., and Johansson, M.: A new climate era in the sub-Arctic: Accelerating climate changes and multiple impacts, Geophys. Res. Lett., 37, L14705, doi:10.1029/2009GL042064, 2010.

Chanton, J. P., Chasar, L., Glaser, P. H., and Siegel, D. I.: Carbon and hydrogen isotopic effects in microbial methane from terrestrial environments, in: Stable isotopes and biosphere-atmosphere interactions: processes and biological controls, edited by: Flanagan, L. B., Ehleringer, J. R., and Pataki, D. E., Elsevier, Amsterdam, 85–105, 2005.

Christensen, T. R., Johansson, T., Åkerman, H. J., Mastepanov, M., Malmer, N., Friborg, T., Crill, P., and Svensson, B. H.: Thawing sub-arctic permafrost: effects on vegetation and methane emissions, Geophys. Res. Lett., 31, L04501, doi:10.1029/2003GL018680, 2004.

Christensen, T. R., Jackowicz-Korczyński, M., Aurela, M., Crill, P., Heliasz, M., Mastepanov, M., and Friborg, T.: Monitoring the multi-year carbon balance of a subarctic palsa mire with micrometeorological techniques, Ambio, 41, 207–217, 2012.

Clauser, C. and Huenges, E.: Thermal conductivity of rocks and minerals, in: Rock Physics & Phase Relations: A Handbook of Physical Constants, Ahrens, T. J., AGU, Washington, DC, 105–126, 1995.

Corbett, J. E., Tfaily, M. M., Burdige, D. J., Cooper, W. T., Glaser, P. H., and Chanton, J. P.: Partitioning pathways of CO_2 production in peatlands with stable carbon isotopes, Biogeochemistry, 114, 327–340, doi:10.1007/s10533-012-9813-1, 2013.

Davis, N.: Permafrost: A Guide to Frozen Ground in Transition, University of Alaska Press, Fairbanks, AK, 2001.

Dorrepaal, E., Toet, S., van Logtestijn, R. S. P., Swart, E., van de Weg, M. J., Callaghan, T. V., and Aerts, R.: Carbon respiration from subsurface peat accelerated by climate warming in the subarctic, Nature, 460, 616–619, 2009.

Frolking, S. and Roulet, N. T.: Holocene radiative forcing impact of northern peatland carbon accumulation and methane emissions, Glob. Change Biol., 13, 1079–1088, 2007.

Frolking, S., Roulet, N., and Fuglestvedt, J.: How northern peatlands influence the Earth's radiative budget: Sustained methane emission versus sustained carbon sequestration, J. Geophys. Res., 111, G01008, doi:10.1029/2005JG000091, 2006.

Frolking, S., Talbot, J., Jones, M., Treat, C. C., Kauffman, J. B., Tuittila, E. S., and Roulet, N. T.: Peatlands in the Earth's 21st century climate system, Environ. Rev., 19, 371–396, 2011.

Fumoto, F., Kobayashi, K., Li, C., Yagi, K., and Hasegawa, T.: Revising a process-based biogeochemistry model (DNDC) to simulate methane emission from rice paddy fields under various residue management and fertilizer regimes, Glob. Change Biol., 14, 382–402, 2008.

Goetz, S. J., Epstein, H. E., Bhatt, U. S., Jia, G. J., Kaplan, J. O., Lischke, H., Yu, Q., Bunn, A., Lloyd, A. H., Alcaraz-Segura, D., Beck, P. S. A., Comiso, J. C., Raynolds, M. K., and Walker,

D. A.: Recent changes in arctic vegetation: satellite observations and simulation model predictions, in: Eurasian arctic land cover and land use in a changing climate, edited by: Gutman, G. and Reissell, A., Springer, Nertherlands, 9–36, 2011.

IPCC: Climate change 2007: the physical science basis, In: Contribution of working group I to the fourth assessment report of the Intergovernmental Panel on Climate Change: "The Physical Science Basis", edited by: Solomon, S., Qin, D., Manning, M., Chen, Z., Marquis, M., Averyt, K. B., Tignor, M., and Miller, H. L., Cambridge University Press, Cambridge, 2007.

Jackowicz-Korczyński, M., Christensen, T. R., Bäckstrand, K., Crill, P. M., Friborg, T., Mastepanov, M., and Ström, L.: Annual cycle of methane emission from a subarctic peatland, J. Geophys. Res., 115, G02009, doi:10.1029/2008JG000913, 2010.

James, M., Lewkowicz, A. G., Smith, S. L., and Miceli, C. M.: Multi-decadal degradation and persistence of permafrost in the Alaska Highway corridor, northwest Canada, Environ. Res. Lett., 8, 045013, doi:10.1088/1748-9326/8/4/045013, 2013.

Johansson, M., Christensen, T. R., Åkerman, J. H., and Callaghan, T. V.: What determines the current presence or absence of permafrost in the torneträsk region, a sub-arctic landscape in northern Sweden, Ambio, 35, 190–197, 2006.

Johansson, T., Malmer, N., Crill, P. M., Friborg, T., Åkerman, J., Mastepanov, M., and Christensen, T. R.: Decadal vegetation changes in a northern peatland, greenhouse gas fluxes and net radiative forcing, Glob. Change Biol., 12, 2352–2369, doi:10.1111/j.1365-2486.2006.01267.x, 2006.

Kirschke, S., Bousquet, P., Ciais, P., Saunois, M., Canadell, J. G., Dlugokencky, E. J., Bergamaschi, P., Bergmann, D., Blake, D. R., Bruhwiler, L., Cameron-Smith, P., Castaldi, S., Chevallier, F., Feng, L., Fraser, A., Heimann, M., Hodson, E. L., Houweling, S., Josse, B., Fraser, P. J., Krummel, P. B., Lamarque, J., Langenfelds, R. L., Le Quere, C., Naik, V., O'Doherty, S., Palmer, P. I., Pison, I., Plummer, D., Poulter, B., Prinn, R. G., Rigby, M., Ringeval, B., Santini, M., Schmidt, M., Shindell, D. T., Simpson, I. J., Spahni, R., Steele, L. P., Strode, S. A., Sudo, K., Szopa, S., van der Werf, G. R., Voulgarakis, A., van Weele, M., Weiss, R. F., Williams, J. E., and Zeng, G.: Three decades of global methane sources and sinks, Nat. Geosci., 6, 813–823, doi:10.1038/NGEO1955, 2013.

Kokfelt, U., Reuss, N., Struyf, E., Sonesson, M., Rundgren, M., Skog, G., Rosén, P., and Hammarlund, D.: Wetland development, permafrost history and nutrient cycling inferred from late Holocene peat and lake sediment records in subarctic Sweden, J. Paleolimnol., 44, 327–342, 2010.

Koven, C. D., Ringeval, B., Friedlingstein, P., Ciais, P., Cadule, P., Khvorostyanov, D., Krinner, G., and Tarnocai, C.: Permafrost carbon-climate feedbacks accelerate global warming, P. Natl. Acad. Sci. USA, 108, 14769–14774, 2011.

Li, C.: Modeling trace gas emissions from agricultural ecosystems, Nutr. Cycl. Agroecos., 58, 259–276, doi:10.1023/A:1009859006242, 2000.

Li, C.: Quantifying greenhouse gas emissions from soils: scientific basis and modeling approach, Soil Sci. Plant Nutr., 53, 344–352, 2007.

Li, C., Frolking, S., and Frolking, T. A.: A model of nitrous oxide evolution from soil driven by rainfall events: 1. Model structure and sensitivity, J. Geophys. Res., 97, 9759–9776, 1992a.

Li, C., Frolking, S., and Frolking, T. A.: A model of nitrous oxide evolution from soil driven by rainfall events: 2. Model applications, J. Geophys. Res., 97, 9777–9783, 1992b.

Li, C., Aber, J., Stange, F., Butterbach-Bahl, K., and Papen, H.: A process-oriented model of N_2O and NO emissions from forest soils: 1. Model development, J. Geophys. Res., 105, 4365–4384, 2000.

Li, C., Salas, W., Zhang, R., Krauter, C., Rotz, A., and Mitloehner, F.: Manure-DNDC: a biogeochemical process model for quantifying greenhouse gas and ammonia emissions from livestock manure systems, Nutr. Cycl. Agroecos., 93, 163–200, doi:10.1007/s10705-012-9507-z, 2012.

Lund, M., Lafleur, P. M., Roulet, N. T., Lindroth, A., Christensen, T. R., Aurela, M., Chojnicki, B. H., Flanagan, L. B., Humphreys, E. R., Laurila, T., Oechel, W. C., Olejnik, J., Rinne, J., Schubert, P., and Nilsson, M. B.: Variability in exchange of CO_2 across 12 northern peatland and tundra sites, Glob. Change Biol., 16, 2436–2448, 2010.

Majorowicz, J. and Wybraniec, S.: New terrestrial heat flow map of Europe after regional paleoclimatic correction application, Int. J. Earth Sci., 100, 881–887, 2011.

Malmer, N. and Wallén, B.: Peat formation and mass balance in subarctic ombrotrophic peatlands around Abisko, northern Scandinavia, Ecol. Bull., 45, 79–92, 1996.

Malmer, N., Johansson, T., Olsrud, M., and Christensen, T. R.: Vegetation, climatic changes and net carbon sequestration in a North-Scandinavian subarctic mire over 30 years, Glob. Change Biol., 11, 1895–1909, 2005.

McGuire, A. D., Anderson, L. G., Christensen, T. R., Dallimore, S., Guo, L., Hayes, D. J., Helmann, M., Lorenson, T. D., Macdonald, R. W., and Roulet, N.: Sensitivity of the carbon cycle in the Arctic to climate change, Ecol. Monogr., 79, 523–555, 2009.

Moriasi, D. N., Arnold, J. G., Van Liew, M. W., Bingner, R. L., Harmel, R. D., and Veith, T. L.: Model evaluation guidelines for systematic quantification of accuracy in watershed simulations, T. ASABE, 50, 885–900, 2007.

Nungesser, M. K.: Modelling microtopography in boreal peatlands: hummocks and hollows, Ecol. Model., 165, 175–207, 2003.

Olefeldt, D. and Roulet, N. T.: Effects of permafrost and hydrology on the composition and transport of dissolved organic carbon in a subarctic peatland complex, J. Geophys. Res., 117, G01005, doi:10.1029/2011JG001819, 2012.

Olefeldt, D., Roulet, N. T., Bergeron, O., Crill, P. M., Bäckstrand, K., and Christensen, T. R.: Net carbon accumulation of a high-latitude permafrost palsa mire similar to permafrost-free peatlands, Geophys. Res. Lett., 39, L03501, doi:10.1029/2011GL050355, 2012.

Olefeldt, D., Turetsky, M. R., Crill, P. M., and McGuire, A. D.: Environmental and physical controls on northern terrestrial methane emissions across permafrost zones, Glob. Change Biol., 19, 589–603, 2013.

Olsrud, M. and Christensen, T. R.: Carbon partitioning in a wet and a semiwet subarctic mire ecosystem based on in situ ^{14}C pulse-labelling, Soil Biol. Biochem., 43, 231–239, 2011.

Öquist, M. G. and Svensson, B. H.: Vascular plants as regulators of methane emissions from a subarctic mire ecosystem, J. Geophys. Res., 107, 4580, doi:10.1029/2001JD001030, 2002.

Payette, S., Delwaide, A., Caccianiga, M., and Beauchemin, M.: Accelerated thawing of subarctic peatland permafrost

over the last 50 years, Geophys. Res. Lett., 31, L18208, doi:10.1029/2004GL020358, 2004.

Paris, J. D., Ciais, P., Rivier, L., Chevallier, F., Dolman, H., Flaud, J. M., Garrec, C., Gerbig, C., Grace, J., Huertas, E., Johannessen, T., Jordan, A., Levin, I., Papale, D., Valentini, R., Watson, A., Vesala, T., and ICOS-PP consortium: Integrated Carbon Observation System, Geophys. Res. Abstr., 14, EGU2012-12397, 2012.

Quinton, W., Hayashi, M., and Chasmer, L.: Permafrost-thaw-induced land-cover change in the Canadian subarctic: implications for water resources, Hydrol. Process., 25, 152–158, 2011.

Riseborough, D., Shiklomanov, N., Etzelmüller, B., Gruber, S., and Marchenko, S.: Recent Advances in Permafrost Modelling, Permafrost Periglac., 19, 137–156, 2008.

Rosswall, T., Flower-Ellis, J. G. K., Johansson, L. G., Jonsson, S., Rydén, B. E., and Sonesson, M.: Stordalen (Abisko), Sweden, Ecol. Bull., 20, 265–294, 1975.

Rydén, B. E.: Climatic representativeness of a project period: epilogue of a tundra study, Ecol. Bull., 30, 55–62, 1980.

Rydén, B. E. and Kostov, L.: Thawing and freezing in tundra soils, Ecol. Bull., 30, 251–281, 1980.

Rydén, B. E., Fors, L., and Kostov, L.: Physical properties of the tundra soil-water system at Stordalen, Abisko, Ecol. Bull., 30, 27–54, 1980.

Sachs, T., Giebels, M., Boike, J., and Kutzbach, L.: Environmental controls of CH_4 emission from polygonal tundra on the microsite scale, Lena River Delta, Siberia, Glob. Change Biol., 16, 3096–3110, 2010.

Schneider von Deimling, T., Meinshausen, M., Levermann, A., Huber, V., Frieler, K., Lawrence, D. M., and Brovkin, V.: Estimating the near-surface permafrost-carbon feedback on global warming, Biogeosciences, 9, 649–665, doi:10.5194/bg-9-649-2012, 2012.

Schuur, E. A. G., Bockheim, J., Canadell, J. G., Euskirchen, E., Field, C. B., Goryachkin, S. V., Hagemann, S., Kuhry, P., Lafleur, P. M., Lee, H., Mazhitova, G., Nelson, F. E., Rinke, A., Romanovsky, V. E., Shiklomanov, N., Tarnocai, C., Venevsky, S., Vogel, J. G., and Zimov, S. A.: Vulnerability of permafrost carbon to climate change: implications for the global carbon cycle, BioScience, 58, 701–714, 2008.

Schuur, E. A. G., Vogel, J. G., Grummer, K. G., Lee, H., Sickman, J. O., and Osterkamp, T. E.: The effect of permafrost thaw on old carbon release and net carbon exchange from tundra, Nature, 459, 556–559, 2009.

Schuur, E. A. G., Benjamin, A., and Permafrost Carbon Network: High risk of permafrost thaw, Nature, 480, 32–33, 2011.

Shine, K. P., Derwent, R. G., Wuebbles, D. F., and Morcrette, J. J.: Radiative forcing of climate, in: Climate Change: The IPCC Scientific Assessment, edited by: Houghton, J. T., Jenkins, G. J., and Ephraums, J. J., Cambridge University Press, Cambridge, UK, 41–68, 1990.

Smith, L. C., Sheng, Y., McDonald, G. M., and Hinzman, L. D.: Disappearing arctic lakes, Science, 308, 1429, doi:10.1126/science.1108142,2005.

Sonesson, M., Jonsson, S., Rosswall, T., and Rydén, B. E.: The Swedish IBP/PT tundra biome project: objectives – planning – site, Ecol. Bull., 30, 7–25, 1980.

Stange, F., Butterbach-Bahl, K., Papen, H., Zechmeister-Boltenster, S., Li, C., and Aber, J.: A process-oriented model of N_2O and NO emissions from forest soils: 2. Sensitivity analysis and validation, J. Geophys. Res., 105, 4385–4398, 2000.

Ström, L. and Christensen, T. R.: Below ground carbon turnover and greenhouse gas exchanges in a sub-arctic wetland, Soil Biol. Biochem., 39, 1689–1698, 2007.

Tarnocai, C., Canadell, J. G., Schuur, E. A. G., Kuhry, P., Mazhitova, G., and Zimov, S.: Soil organic carbon pools in the northern circumpolar permafrost region, Global Biogeochem. Cy., 23, GB2023, doi:10.1029/2008GB003327, 2009.

Waelbroeck, C.: Climate-soil processes in the presence of permafrost: a systems modelling approach, Ecol. Model., 69, 185–225, 1993.

Wania, R., Ross, I., and Prentice, I. C.: Integrating peatlands and permafrost into a dynamicglobal vegetation model: 1. Evaluation and sensitivity of physical land surface processes, Global Biogeochem. Cy., 23, GB3014, doi:10.1029/2008GB003412, 2009a.

Wania, R., Ross, I., and Prentice, I. C.: Integrating peatlands and permafrost into a dynamic global vegetation model: 2. Evaluation and sensitivity of vegetation and carbon cycle processes, Global Biogeochem. Cy., 23, GB3015, doi:10.1029/2008GB003413, 2009b.

Whiting, G. J. and Chanton, J. P.: Greenhouse carbon balance of wetlands: methane emission versus carbon sequestration, Tellus B, 53, 521–528, 2001.

Williams, P. J. and Smith, M. W.: The Frozen Earth: Fundamentals of Geocryology, Cambridge University Press, Cambridge, UK, 1989.

Willmott, C. J.: Some comments on the evaluation of model performance, B. AM. Meteorol. Soc., 63, 1309–1313, 1982.

Willmott, C. J., Ackleson, S. G., Davis, R. E., Feddema, J. J., Klink, K. M., Legates, D. R., O'Donnell, J., and Rowe, C. M.: Statistics for the evaluation and comparison of models, J. Geophys. Res., 90, 8995–9005, 1985.

Yu, Z., Loisel, J., Brosseau, D. P., Beilman, D. W., and Hunt, S. J.: Global peatland dynamics since the Last Glacial Maximum, Geophys. Res. Lett., 37, L13402, doi:10.1029/2010GL043584, 2010.

Zhang, Y., Li, C., Trettin, C. C., Li, H., and Sun, G.: An integrated model of soil, hydrology and vegetation for carbon dynamics in wetland ecosystems, Global Biogeochem. Cy., 16, 1061, doi:10.1029/2001GB001838, 2002.

Zhang, Y., Chen, W., and Cihlar, J.: A process-based model for quantifying the impact of climate change on permafrost thermal regimes, J. Geophys. Res., 108, 4695, doi:10.1029/2002JD003354, 2003.

Zhang, Y., Chen, W., Smith, S. L., Riseborough, D. W., and Cihlar, J.: Soil temperature in Canada during the twentieth century: complex responses to atmospheric climate change, J. Geophys. Res., 110, D03112, doi:10.1029/2004JD004910, 2005.

Zhang, Y., Sachs, T., Li, C., and Boike, J.: Upscaling methane fluxes from closed chambers to eddy covariance based on a permafrost biogeochemistry integrated model, Glob. Change Biol., 18, 1428–1440, doi:10.1111/j.1365-2486.2011.02587.x, 2012.

Zhang, Y., Wang, X., Fraser, R., Olthof, I., Chen, W., Mclennan, D., Ponomarenko, S., and Wu, W.: Modelling and mapping climate change impacts on permafrost at high spatial resolution for an Arctic region with complex terrain, The Cryosphere, 7, 1121–1137, doi:10.5194/tc-7-1121-2013, 2013.

Zhuang, Q., Romanovsk, V. E., and McGuire, A. D.: Incorporation of a permafrost model into a large-scale ecosystem model: Evaluation of temporal and spatial scaling issues in simulating soil thermal dynamics, J. Geophys. Res., 106, 33649–33670, 2001.

Zhuang, Q., Melillo, J. M., Kicklighter, D. W., Prinn, R. G., McGuire, A. D., Steudler, P. A., Felzer, B. S., and Hu, S.: Methane fluxes between terrestrial ecosystems and the atmosphere at northern high latitudes during the past century: a retrospective analysis with a process-based biogeochemistry model, Global Biogeochem. Cy., 18, GB3010, doi:10.1029/2004GB002239, 2004.

Zhuang, Q., Melillo, J. M., Sarofim, M. C., Kicklighter, D. W., McGuire, A. D., Felzer, B. S., Sokolov, A., Prinn, R. G., Steudler, P. A., and Hu, S.: CO_2 and CH_4 exchanges between land ecosystems and the atmosphere in northern high latitudes over the 21st century, Geophys. Res. Lett., 33, L17403, doi:10.1029/2006GL026972, 2006.